Design of Frequency Hopping Waveforms With Good Correlation Properties for Joint MIMO Radar and Communications

Yimeng An, Yongzhe Li, Xiaonan Xu, and Ran Tao
School of Information and Electronics, Beijing Institute of Technology, 100081 Beijing, China
Emails: yimeng.an@bit.edu.cn, lyz@ieee.org, xiaonan.xu@bit.edu.cn, rantao@bit.edu.cn

***Abstract*—In this paper, we design the multiple frequency-hopping (FH) waveforms for the joint radar and communications, aiming to improve correlation properties of waveforms and meanwhile to guarantee high-quality information transmission. To this end, we first establish an appropriate model for the FH waveforms. Then, we exploit the frequency diversity of waveforms to implement information embedding (IE) in the fast-time domain from the communication side, and utilize the flexibility of initial phases of waveforms to reduce the integrated sidelobe level (ISL) of FH waveforms from the radar point of view. We propose the waveform design that minimizes ISL under constraints of fast-time IE and constant-modulus waveform property, which is formulated as a non-convex optimization problem. To solve it, we explore the inherent algebraic structures and apply elementary properties to transform its objective function into a tractable form. Our major contributions also lie in elaborating a series of proper majorants for the reformulated objective function via majorization-minimization technique, which helps us to derive closed-form solutions for iterations. Simulation results verify the effectiveness of our proposed design.**

***Index Terms*—Frequency hopping, information embedding, integrated sidelobe level, joint radar and communications, waveform design.**

I. Introduction

The joint radar and communications (JRC), which aims to tackle the issues of frequency spectrum congestion and competition, has become a hot research topic in recent years [1]–[3]. Among the relevant research, the JRC [1]–[11] mainly focus on collaborative design and co-design from the perspective of implementation. The former category suppresses or manages the interference between radar and communications with independent transmitters and overlapping bands in a collaborative manner [3]–[5], while the latter enables radar and communications to share the spectral and hardware resources in an integration manner [6]–[11]. Since the co-designed JRC can reduce the size, power consumption, and cost, the latter category has attracted significant interest over the past decade. To integrate both radar and communication functions into one platform, some approaches are developed to embed communication information into frequency-hopping (FH) [6]–[8], frequency-modulated continuous wave [9], [10], or orthogonal frequency division multiplexing [11] waveform emissions of radar in JRC.

When communication information is embedded into FH waveforms, the JRC benefits from the excellent anti-interference capability [10] and low probability of intercept [12], which has therefore been studied extensively [12]–[17]. To implement high-rate information transmission, some information embedding (IE) strategies based on fast-time waveform modulation scheme, such as code shift keying [12], phase shift keying [13], or frequency index modulations [14], have been investigated. However, these IE strategies lead to high correlations of FH waveforms, which prevents the extraction of potential targets with low attenuation. Aiming to address this issue, the work of [15] utilizes the interleaving technique to optimize the mapped communication symbols. Although it can effectively reduce the auto-correlation level of FH waveforms, it comes at the cost of increased cross-correlations. To further improve correlations of FH waveforms, the codebook optimizations are studied [16], [17]. Unfortunately, they solve the corresponding optimization problems using genetic or exhaustive search algorithms with high computational complexities. These motivate us to develop an advanced FH waveform design with good correlation properties and low computational complexity for the JRC.

In this paper, we focus on the multi-FH waveform design for the JRC. Our goal is to simultaneously achieve good correlation properties of FH waveforms and high-quality communication transmission. To facilitate the design, we first establish an appropriate model for FH waveforms. Then, we exploit the frequency diversity of waveforms to embed information in the fast-time domain for the communication side, and utilize the flexibility of their initial phases to reduce the integrated sidelobe level (ISL) for the radar side. Based on this, we formulate the proposed waveform design as a non-convex optimization problem, which minimizes the ISL under the constraints on fast-time IE and constant-modulus property. To solve it, we transform the objective function into a tractable form by exploring its inherent algebraic structures and properties. Our major contributions also lie in developing an algorithm that iterates with closed-form solutions after elaborating a series of proper majorants for the newly obtained objective function within the majorization-minimization framework [18]. Simulations verify the effectiveness of our proposed design.

Notations: We use $\otimes$, $\odot$, $\bigtriangledown$, $\succeq$, $(\cdot)^*$, $(\cdot)^{\mathrm{T}}$, $(\cdot)^{\mathrm{H}}$, $|\cdot|$, $\|\cdot\|$, $\mathrm{vec}(\cdot)$, $\arg(\cdot)$, $\lambda_{\max}(\cdot)$, $\mathcal{O}(\cdot)$, $\Re\{\cdot\}$, $\mathfrak{D}\{\cdot\}$, and $\max\{\cdot\}$ to denote the Kronecker product, Hadamard product, gradient operations, generalized inequality between matrices, conjugation, transpose, Hermitian transpose, modulus, Euclidean norm, column-wise vectorization, argument of a complex value,

This work was supported in part by the National Natural Science Foundation of China (NSFC) under grants 62271054 and U21A20456.

largest eigenvalue of a matrix, order of complexity, real part, diagonalization, and maximum value, respectively. In addition, $[\cdot]_{q,n}$ denotes the (q,n)-th element of a matrix, $\mathbf{I}_M$ is an $M\times M$ identity matrix, and $\mathbf{1}_M$ is an $M\times 1$ vector with all elements equal to 1.

II. Signal Model

Consider a JRC system with multi-FH waveform transmission, which simultaneously performs both radar and communications functions through one platform. The JRC launches in total M FH waveforms consisting of Q sub-pulses within one pulse. We denote Δ_f and $\Delta_t = 1/\Delta_f$ as the frequency step and sub-pulse duration, respectively. The m-th baseband FH signal can be expressed as

$$s_m(t)=\sum_{q=1}^{Q}\exp\big\{j(\psi_{m,q}+2\pi c_{m,q}\Delta_f t)\big\}\mathrm{rect}\big(t-(q-1)\Delta_t\big) \tag{1}$$

where $c_{m,q}$ is the FH code selected from the set $\mathbb{S}\triangleq\{1,...,N\}$ within the q-th sub-pulse for the m-th waveform, $\psi_{m,q}$ is the initial phase which arbitrarily ranges between 0 and 2π, and rect$(\cdot)$ is a window function which equals 1 only if the argument falls within $[0,\Delta_t)$ and otherwise is 0. Note that to ensure that the cross-correlations of waveforms are zero at zero-time lag, the selected FH codes for different waveforms within each sub-pulse are distinct, i.e., $c_{m,q}\neq c_{m',q},\ m\neq m',\forall q\in\{1,...,Q\}$.

After sampling the baseband FH signal via the proper sampling interval t_s, the discrete form of (1) can be expressed as follows

$$\begin{aligned}s_m(p)=&\sum_{q=1}^{Q}\exp\big\{j\big(\psi_{m,q}+2\pi c_{m,q}\Delta_f(p-1)t_\mathrm{s}\big)\big\}\\&\times\mathrm{rect}\big((p-1)t_\mathrm{s}-(q-1)\Delta_t\big),\ p\in\{1,...,QL\}\end{aligned} \tag{2}$$

where $L\triangleq\Delta_t/t_\mathrm{s}$ is the number of discrete samples within one sub-pulse.

Let us introduce the vectors $\mathbf{d}\triangleq[0,2\pi/L,\ldots,2\pi(L-1)/L]^\mathrm{T}\in\mathbb{R}^{L\times 1}$, $\mathbf{c}_m\triangleq[c_{m,1},...,c_{m,Q}]^\mathrm{T}\in\mathbb{R}^{Q\times 1}$, and $\boldsymbol{\psi}_m\triangleq\big\{\exp\{j\psi_{m,1}\},...,\exp\{j\psi_{m,Q}\}\big\}^\mathrm{T}\in\mathbb{C}^{Q\times 1}$. Based on these vectors, we can rewrite (2) into the form given as follows

$$\mathbf{s}_m=\exp\big\{(j\mathbf{c}_m)\otimes\mathbf{d}\big\}\odot(\boldsymbol{\psi}_m\otimes\mathbf{1}_L). \tag{3}$$

From the perspective of MIMO radar, the set of M waveforms is expected to have good correlation properties and perfect mutual orthogonality to each other, so that targets at range bins of interest can be easily extracted without attenuation. Toward this end, the ISL which characterizes the auto- and cross-correlations of waveforms is commonly used, which can be expressed as the following form

$$\zeta=\sum_{m=1}^{M}\sum_{\substack{p=-QL+1\\p\neq 0}}^{QL-1}|r_{mm}(p)|^2+\sum_{m=1}^{M}\sum_{\substack{m'=1\\m'\neq m}}^{M}\sum_{p=-QL+1}^{QL-1}|r_{mm'}(p)|^2 \tag{4}$$

where $r_{mm'}(p)\triangleq\sum_{l=p+1}^{QL}s_m(l)s_{m'}^*(l-p)=\big(r_{m'm}(-p)\big)^*$, $p\in\{1,\ldots,QL-1\}$ denotes the cross-correlation between the m-th and m'-th waveforms at the p-th time lag.

From the perspective of communications, the high-rate IE is of interest, which can be implemented by waveform modulation in the fast-time domain. To this end, we here apply frequency index modulation to choose FH code from the set $\mathbb{S}$ for each waveform within each sub-pulse, which enables the mapping relationship given as follows

$$\mathbf{c}_m=\mathbf{U}_m\mathbf{h},\ m\in\{1,...,M\} \tag{5}$$

where the vector $\mathbf{h}\triangleq[1,\ldots,N]^\mathrm{T}\in\mathbb{R}^{N\times 1}$ is composed of all available FH codes, $\mathbf{U}_m\in\mathbb{R}^{Q\times N}$ is the selection matrix whose (q,n)-th element is chosen from $\{0,1\}$ to record the selection of the FH code n for the m-th waveform within Q sub-pulses. Note that the M selection matrices during each pulse satisfy the condition $[\mathbf{U}_m]_{q,n}\neq[\mathbf{U}_{m'}]_{q,n},\ m\neq m';q\in\{1,...,Q\};n\in\{1,...,N\}$, thereby ensuring that the cross-correlations of waveforms are zero at zero time lag. For this IE strategy, the user can obtain the matrices $\{\mathbf{U}_m\}_{m=1}^M$ via the maximal-likelihood detection.

Overall, the JRC that integrates both radar and communication functions into one platform can be implemented via waveform design under the constraint of IE. Our goal here is to obtain good correlation properties of multiple waveforms from the radar side, and meanwhile, to achieve high-quality information transmission from the communication side.

III. The FH Waveform Design With IE

In this section, we propose a novel method to design multi-FH waveforms with low ISL and high-quality communication for the JRC. Based on the signal model above, the FH waveform design, which minimizes ISL under the constraints of constant-modulus property and fast-time IE with frequency index modulation, can be formulated as

$$\min_{\{\mathbf{s}_m,\boldsymbol{\psi}_m\}_{m=1}^M}\ \zeta \tag{6a}$$

$$\text{s.t.}\quad |\boldsymbol{\psi}_m(q)|=1,\ q\in\{1,\ldots,Q\};m\in\{1,\ldots,M\} \tag{6b}$$

$$\mathbf{s}_m=\exp\big\{(j\mathbf{U}_m\mathbf{h})\otimes\mathbf{d}\big\}\odot(\boldsymbol{\psi}_m\otimes\mathbf{1}_L),\quad m\in\{1,\ldots,M\} \tag{6c}$$

where the objective function (6a) formulates the ISL ζ that has been defined in (4), the constraint (6b) guarantees the constant-modulus property of FH waveform, and the constraint (6c) obtained by substituting (5) to (3) guarantees the high-rate IE with the predetermined selection matrix $\mathbf{U}_m$. Note that the optimization problem (6) is non-convex and difficult to solve, for which an efficient solution is to be developed.

Before proceeding with (6), we need to introduce several new vectors and matrices to transform the ISL ζ into the frequency domain [18]. To this end, we store all vectors $\{\boldsymbol{\psi}_m\}_{m=1}^M$ and $\{\mathbf{s}_m\}_{m=1}^M$, and also matrices $\{\mathbf{U}_m\}_{m=1}^M$ into $\boldsymbol{\psi}\triangleq[\boldsymbol{\psi}_1^\mathrm{T},\ldots,\boldsymbol{\psi}_M^\mathrm{T}]^\mathrm{T}\in\mathbb{C}^{MQ\times 1}$, $\mathbf{s}\triangleq\big[\mathbf{s}_1^\mathrm{T},\ldots,\mathbf{s}_M^\mathrm{T}\big]^\mathrm{T}\in\mathbb{C}^{MQL\times 1}$, and $\mathbf{U}\triangleq[\mathbf{U}_1^\mathrm{T},\ldots,\mathbf{U}_M^\mathrm{T}]^\mathrm{T}\in\mathbb{R}^{MQ\times N}$, respectively.

Based on these new vectors and matrix, and also the constraint (6c), we can rewrite the overall waveform vector $\mathbf{s}$ as $\mathbf{s}=\mathbf{C}\boldsymbol{\psi}$ with $\mathbf{C}\triangleq\mathfrak{D}\big\{\exp\{(j\mathbf{U}\mathbf{h})\otimes\mathbf{d}\}\big\}(\mathbf{I}_{MQ}\otimes\mathbf{1}_L)\in\mathbb{C}^{MQL\times MQ}$. Introducing the vector $\mathbf{a}_p\triangleq\big[1,\exp\{j\omega_p\},\ldots,\exp\{j(QL-1)\omega_p\}\big]^{\mathrm{T}}\in\mathbb{C}^{QL\times 1}$ with $\omega_p\triangleq\pi p/(QL)$ and the matrix $\mathbf{A}_p\triangleq\mathbf{I}_M\otimes\mathbf{a}_p\in\mathbb{C}^{MQL\times M}$ with $p\in\{1,\ldots,2QL\}$, the ISL ζ in (4), after transforming into the frequency domain, can be rewritten as follows

$$\begin{aligned}\zeta&=\frac{1}{2QL}\sum_{p=1}^{2QL}\big((\mathbf{s}^{\mathrm{H}}\mathbf{A}_p\mathbf{A}_p^{\mathrm{H}}\mathbf{s})^2-2QL\mathbf{s}^{\mathrm{H}}\mathbf{A}_p\mathbf{A}_p^{\mathrm{H}}\mathbf{s}+MQ^2L^2\big)\\&=\frac{1}{2QL}\sum_{p=1}^{2QL}\big((\boldsymbol{\psi}^{\mathrm{H}}\mathbf{C}^{\mathrm{H}}\mathbf{A}_p\mathbf{A}_p^{\mathrm{H}}\mathbf{C}\boldsymbol{\psi})^2-2QL\boldsymbol{\psi}^{\mathrm{H}}\mathbf{C}^{\mathrm{H}}\mathbf{A}_p\mathbf{A}_p^{\mathrm{H}}\mathbf{C}\boldsymbol{\psi}\\&\qquad+MQ^2L^2\big)\quad(7)\end{aligned}$$

Note that the second term on the right-hand side of (7) is constant, which can be proved by the facts that $\|\boldsymbol{\psi}\|^2=MQ$, $\mathbf{C}^{\mathrm{H}}\mathbf{C}=L\mathbf{I}_{MQ}$, and $\sum_{p=1}^{2QL}\mathbf{A}_p\mathbf{A}_p^{\mathrm{H}}=2QL\mathbf{I}_{MQL}$.

Substituting (7) into (6) and ignoring the constant terms, the original optimization problem can be rewritten as

$$\begin{aligned}\min_{\boldsymbol{\psi}}\quad&\sum_{p=1}^{2QL}(\boldsymbol{\psi}^{\mathrm{H}}\mathbf{C}^{\mathrm{H}}\mathbf{A}_p\mathbf{A}_p^{\mathrm{H}}\mathbf{C}\boldsymbol{\psi})^2&(8a)\\\text{s.t.}\quad&|\boldsymbol{\psi}(q')|=1,\ q'\in\{1,\ldots,MQ\}&(8b)\end{aligned}$$

where the objective function (8a) takes a quartic form with respect to $\boldsymbol{\psi}$. Introducing the matrix $\boldsymbol{\Psi}\triangleq\boldsymbol{\psi}\boldsymbol{\psi}^{\mathrm{H}}$ and using the property $\boldsymbol{\psi}^{\mathrm{H}}\mathbf{C}^{\mathrm{H}}\mathbf{A}_p\mathbf{A}_p^{\mathrm{H}}\mathbf{C}\boldsymbol{\psi}=(\mathrm{vec}(\mathbf{C}\boldsymbol{\Psi}\mathbf{C}^{\mathrm{H}}))^{\mathrm{H}}\mathrm{vec}(\mathbf{A}_p\mathbf{A}_p^{\mathrm{H}})$, the problem (8) can be further rewritten as

$$\begin{aligned}\min_{\boldsymbol{\Psi}}\quad&(\mathrm{vec}(\mathbf{C}\boldsymbol{\Psi}\mathbf{C}^{\mathrm{H}}))^{\mathrm{H}}\boldsymbol{\Phi}\mathrm{vec}(\mathbf{C}\boldsymbol{\Psi}\mathbf{C}^{\mathrm{H}})&(9a)\\\text{s.t.}\quad&\boldsymbol{\Psi}=\boldsymbol{\psi}\boldsymbol{\psi}^{\mathrm{H}}&(9b)\\&|\boldsymbol{\psi}(q')|=1,\ q'\in\{1,\ldots,MQ\}&(9c)\end{aligned}$$

where $\boldsymbol{\Phi}\triangleq\sum_{p=1}^{2QL}\mathrm{vec}(\mathbf{A}_p\mathbf{A}_p^{\mathrm{H}})(\mathrm{vec}(\mathbf{A}_p\mathbf{A}_p^{\mathrm{H}}))^{\mathrm{H}}$. To solve the problem (9), we here apply the majorization-minimization technique [18] to elaborate a proper majorant for the objective function (9a). Before proceeding with (9a), we present the following general result about majorization.

Lemma 1 [18]: If a real-valued function $f(\mathbf{x})$ is second-order differentiable with respect to a complex variable $\mathbf{x}$, and there is a matrix $\mathbf{G}\succeq 0$ such that the second-order derivative $\bigtriangledown^2 f(\mathbf{x})$ satisfies the generalized inequality $\bigtriangledown^2 f(\mathbf{x})\preceq\mathbf{G}$ for all $\mathbf{x}$, then for each point $\mathbf{x}_0$, the following convex quadratic function

$$\begin{aligned}g(\mathbf{x})=f(\mathbf{x}_0)+\frac{1}{2}(\mathbf{x}-\mathbf{x}_0)^{\mathrm{H}}\mathbf{G}(\mathbf{x}-\mathbf{x}_0)\\+\Re\big\{\bigtriangledown^{\mathrm{H}}f(\mathbf{x}_0)(\mathbf{x}-\mathbf{x}_0)\big\}\quad(10)\end{aligned}$$

majorizes $f(\mathbf{x})$ at $\mathbf{x}_0$.

Applying the majorization result (10) presented above, and setting $\mathbf{G}\triangleq\lambda_{\max}(\boldsymbol{\Phi})\mathbf{I}_{M^2Q^2L^2}$, the objective function (9a) can be majorized as follows

$$\begin{aligned}g_1(\boldsymbol{\Psi},\boldsymbol{\Psi}^{(k)})=&(\mathrm{vec}(\mathbf{C}\boldsymbol{\Psi}^{(k)}\mathbf{C}^{\mathrm{H}}))^{\mathrm{H}}\big(\tfrac{\lambda_{\max}(\boldsymbol{\Phi})}{2}\mathbf{I}_{M^2Q^2L^2}-\boldsymbol{\Phi}\big)\\&\times\mathrm{vec}(\mathbf{C}\boldsymbol{\Psi}^{(k)}\mathbf{C}^{\mathrm{H}})+2\Re\big\{(\mathrm{vec}(\mathbf{C}\boldsymbol{\Psi}\mathbf{C}^{\mathrm{H}}))^{\mathrm{H}}\\&\times\big(\boldsymbol{\Phi}-\tfrac{\lambda_{\max}(\boldsymbol{\Phi})}{2}\mathbf{I}_{M^2Q^2L^2}\big)\mathrm{vec}(\mathbf{C}\boldsymbol{\Psi}^{(k)}\mathbf{C}^{\mathrm{H}})\big\}\\&+\tfrac{\lambda_{\max}(\boldsymbol{\Phi})}{2}(\mathrm{vec}(\mathbf{C}\boldsymbol{\Psi}\mathbf{C}^{\mathrm{H}}))^{\mathrm{H}}\mathrm{vec}(\mathbf{C}\boldsymbol{\Psi}\mathbf{C}^{\mathrm{H}})\quad(11)\end{aligned}$$

where we use the superscript $(\cdot)^{(k)}$ to mark the corresponding update at the k-th iteration, and the maximum eigenvalue of $\boldsymbol{\Phi}$ is $\lambda_{\max}(\boldsymbol{\Phi})=2MQ^2L^2$. Utilizing the property $(\mathrm{vec}(\mathbf{C}\boldsymbol{\Psi}\mathbf{C}^{\mathrm{H}}))^{\mathrm{H}}\mathrm{vec}(\mathbf{C}\boldsymbol{\Psi}\mathbf{C}^{\mathrm{H}})=M^2Q^2L^2$, the first and third terms of (11) are proved to be constant. After ignoring constant terms, the majorant for (9), denoted as obj, can be given by

$$\mathrm{obj}=(\mathrm{vec}(\mathbf{C}\boldsymbol{\Psi}\mathbf{C}^{\mathrm{H}}))^{\mathrm{H}}\big(\boldsymbol{\Phi}-MQ^2L^2\mathbf{I}_{M^2Q^2L^2}\big)\mathrm{vec}(\mathbf{C}\boldsymbol{\Psi}^{(k)}\mathbf{C}^{\mathrm{H}})\quad(12)$$

Using the facts $\mathrm{vec}(\mathbf{A}_p\mathbf{A}_p^{\mathrm{H}})=(\mathbf{A}_p^{\mathrm{T}}\otimes\mathbf{I}_{MQL})^{\mathrm{H}}\mathrm{vec}(\mathbf{A}_p)$ and $\mathrm{vec}(\mathbf{C}\boldsymbol{\Psi}\mathbf{C}^{\mathrm{H}})=((\mathbf{C}^*\boldsymbol{\psi}^*)\otimes\mathbf{C})\boldsymbol{\psi}$, and also the mixed product property of the Kronecker product, (12) can be derived as

$$\begin{aligned}\mathrm{obj}=\sum_{p=1}^{2QL}&\boldsymbol{\psi}^{\mathrm{H}}\big((\boldsymbol{\psi}^{\mathrm{T}}\mathbf{C}^{\mathrm{T}}\mathbf{A}_p^*)\otimes\mathbf{C}^{\mathrm{H}}\big)\mathrm{vec}(\mathbf{A}_p)(\mathrm{vec}(\mathbf{A}_p))^{\mathrm{H}}\\&\times\big((\mathbf{A}_p^{\mathrm{T}}\mathbf{C}^*(\boldsymbol{\psi}^{(k)})^*)\otimes\mathbf{C}\big)\boldsymbol{\psi}^{(k)}-MQ^2L^4\\&\times\boldsymbol{\psi}^{\mathrm{H}}\big((\boldsymbol{\psi}^{\mathrm{T}}(\boldsymbol{\psi}^{(k)})^*)\otimes\mathbf{I}_{MQ}\big)\boldsymbol{\psi}^{(k)}.\quad(13)\end{aligned}$$

Since the equality $\big((\boldsymbol{\psi}^{\mathrm{T}}\mathbf{C}^{\mathrm{T}}\mathbf{A}_p^*)\otimes\mathbf{C}^{\mathrm{H}}\big)\mathrm{vec}(\mathbf{A}_p)=\mathbf{C}^{\mathrm{H}}\mathbf{A}_p\mathbf{A}_p^{\mathrm{H}}\mathbf{C}\boldsymbol{\psi}$ holds, the objective function (13) can be further expressed as

$$\begin{aligned}\mathrm{obj}=\sum_{p=1}^{2QL}&\boldsymbol{\psi}^{\mathrm{H}}\mathbf{C}^{\mathrm{H}}\mathbf{A}_p\big((\boldsymbol{\psi}^{(k)})^{\mathrm{H}}\mathbf{C}^{\mathrm{H}}\mathbf{A}_p\mathbf{A}_p^{\mathrm{H}}\mathbf{C}\boldsymbol{\psi}^{(k)}\big)\\&\times\mathbf{A}_p^{\mathrm{H}}\mathbf{C}\boldsymbol{\psi}-MQ^2L^4\boldsymbol{\psi}^{\mathrm{H}}\big(\boldsymbol{\psi}^{(k)}(\boldsymbol{\psi}^{(k)})^{\mathrm{H}}\big)\boldsymbol{\psi}.\quad(14)\end{aligned}$$

Introducing the matrices $\mathbf{A}\triangleq[\mathbf{A}_1,\ldots,\mathbf{A}_{2QL}]\in\mathbb{C}^{MQL\times 2MQL}$ and $\boldsymbol{\Gamma}^{(k)}\triangleq\mathfrak{D}\big\{\|\mathbf{A}_1^{\mathrm{H}}\mathbf{s}^{(k)}\|^2\mathbf{1}_M^{\mathrm{T}},\ldots,\|\mathbf{A}_{2QL}^{\mathrm{H}}\mathbf{s}^{(k)}\|^2\mathbf{1}_M^{\mathrm{T}}\big\}$, the objective function (14) can be simplified as

$$\mathrm{obj}=\boldsymbol{\psi}^{\mathrm{H}}\big(\mathbf{C}^{\mathrm{H}}\mathbf{A}\boldsymbol{\Gamma}^{(k)}\mathbf{A}^{\mathrm{H}}\mathbf{C}-MQ^2L^4\boldsymbol{\psi}^{(k)}(\boldsymbol{\psi}^{(k)})^{\mathrm{H}}\big)\boldsymbol{\psi}\quad(15)$$

Utilizing (15), we can express the majorized problem for (9) as follows

$$\begin{aligned}\min_{\boldsymbol{\psi}}\quad&\boldsymbol{\psi}^{\mathrm{H}}\big(\mathbf{C}^{\mathrm{H}}\mathbf{A}\boldsymbol{\Gamma}^{(k)}\mathbf{A}^{\mathrm{H}}\mathbf{C}-MQ^2L^4\boldsymbol{\psi}^{(k)}(\boldsymbol{\psi}^{(k)})^{\mathrm{H}}\big)\boldsymbol{\psi}&(16a)\\\text{s.t.}\quad&|\boldsymbol{\psi}(q')|=1,\ q'\in\{1,\ldots,MQ\}&(16b)\end{aligned}$$

where (16a) takes a quadratic form with respect to $\boldsymbol{\psi}$.

To tackle the problem (16), we also apply the majorization result (10) mentioned above. Selecting $\mathbf{G}\triangleq\mu_{\max}^{(k)}\mathbf{C}^{\mathrm{H}}\mathbf{A}\mathbf{A}^{\mathrm{H}}\mathbf{C}$ with $\mu_{\max}^{(k)}\triangleq\max\{\boldsymbol{\Gamma}^{(k)}\}$, the objective function (16a) can be majorized as the following form

$$\begin{aligned}g_2(\boldsymbol{\psi},\boldsymbol{\psi}^{(k)})=&\tfrac{\mu_{\max}^{(k)}}{2}\boldsymbol{\psi}^{\mathrm{H}}\mathbf{C}^{\mathrm{H}}\mathbf{A}\mathbf{A}^{\mathrm{H}}\mathbf{C}\boldsymbol{\psi}+(\boldsymbol{\psi}^{(k)})^{\mathrm{H}}\big(MQ^2L^4\boldsymbol{\psi}^{(k)}\\&\times(\boldsymbol{\psi}^{(k)})^{\mathrm{H}}+\tfrac{\mu_{\max}^{(k)}}{2}\mathbf{C}^{\mathrm{H}}\mathbf{A}\mathbf{A}^{\mathrm{H}}\mathbf{C}-\mathbf{C}^{\mathrm{H}}\mathbf{A}\boldsymbol{\Gamma}^{(k)}\mathbf{A}^{\mathrm{H}}\mathbf{C}\big)\\&\times\boldsymbol{\psi}^{(k)}+2\Re\big\{\boldsymbol{\psi}^{\mathrm{H}}\big(\mathbf{C}^{\mathrm{H}}\mathbf{A}\boldsymbol{\Gamma}^{(k)}\mathbf{A}^{\mathrm{H}}\mathbf{C}-MQ^2L^4\\&\times\boldsymbol{\psi}^{(k)}(\boldsymbol{\psi}^{(k)})^{\mathrm{H}}-\tfrac{\mu_{\max}^{(k)}}{2}\mathbf{C}^{\mathrm{H}}\mathbf{A}\mathbf{A}^{\mathrm{H}}\mathbf{C}\big)\boldsymbol{\psi}^{(k)}\big\}\quad(17)\end{aligned}$$

TABLE I: ISL comparisons of the tested methods versus numbers of waveforms and sub-pulses.

	$M=2$				$M=3$				$M=4$				$M=5$			
	$Q=15$	$Q=30$	$Q=60$	$Q=90$	$Q=15$	$Q=30$	$Q=60$	$Q=90$	$Q=15$	$Q=30$	$Q=60$	$Q=90$	$Q=15$	$Q=30$	$Q=60$	$Q=90$
FHCS	55.84	63.09	71.38	76.49	60.90	69.22	78.04	83.37	64.79	73.52	82.18	87.40	68.24	76.79	85.47	90.73
PBAL	52.92	60.46	68.55	73.27	56.86	64.05	71.76	76.72	61.24	68.54	75.75	80.57	64.87	71.91	79.05	83.60
POCS	51.51	57.56	63.52	67.00	55.04	61.10	67.15	70.76	59.59	65.66	71.72	75.34	63.20	69.21	75.35	78.89
Proposed	49.16	55.12	61.06	64.53	52.89	58.84	64.82	68.31	57.68	63.62	69.59	73.11	61.39	67.35	73.34	76.85

Algorithm 1 The Proposed Waveform Design Algorithm.

1: Initialization: $\boldsymbol{\psi}^{(0)}$, $k \leftarrow 0$
2: **repeat**
3: $\quad \mathbf{s}^{(k)} = \mathbf{C}\boldsymbol{\psi}^{(k)}$
4: $\quad \boldsymbol{\Gamma}^{(k)} = \mathfrak{D}\{\|\mathbf{A}_1^{\mathrm{H}}\mathbf{s}^{(k)}\|^2\mathbf{1}_M^{\mathrm{T}}, \ldots, \|\mathbf{A}_{2QL}^{\mathrm{H}}\mathbf{s}^{(k)}\|^2\mathbf{1}_M^{\mathrm{T}}\}$
5: $\quad \mu_{\max}^{(k)} = \max\{\boldsymbol{\Gamma}^{(k)}\}$
6: $\quad \mathbf{z}^{(k)} = \big(\mathbf{C}^{\mathrm{H}}\mathbf{A}(\frac{\mu_{\max}^{(k)}}{2}\mathbf{I}_{2MQL} - \boldsymbol{\Gamma}^{(k)})\mathbf{A}^{\mathrm{H}}\mathbf{C} + M^2Q^3L^4\mathbf{I}_{MQ}\big)\boldsymbol{\psi}^{(k)}$
7: $\quad \boldsymbol{\psi}^{(k+1)} = \exp\{j \cdot \arg(\mathbf{z}^{(k)})\}$
8: $\quad k \leftarrow k+1$
9: **until** convergence

where the first and second terms on the right-hand side of (17) are constant, which can be obtained by the properties $\mathbf{A}\mathbf{A}^{\mathrm{H}} = 2QL\mathbf{I}_{MQL}$, $\mathbf{C}^{\mathrm{H}}\mathbf{C} = L\mathbf{I}_{MQ}$, and $\boldsymbol{\psi}^{\mathrm{H}}\boldsymbol{\psi} = MQ$. Until now, the majorized problem for (16) can be expressed as

$$\min_{\boldsymbol{\psi}} \quad -\boldsymbol{\psi}^{\mathrm{H}}\mathbf{z}^{(k)} \tag{18a}$$

$$\text{s.t.} \quad |\boldsymbol{\psi}(q')| = 1, \ q' \in \{1, \ldots, MQ\} \tag{18b}$$

whose closed-form solution is obtained by

$$\boldsymbol{\psi} = \exp\{j \cdot \arg(\mathbf{z}^{(k)})\} \tag{19}$$

where

$$\mathbf{z}^{(k)} \triangleq \big(\mathbf{C}^{\mathrm{H}}\mathbf{A}(\tfrac{\mu_{\max}^{(k)}}{2}\mathbf{I}_{2MQL} - \boldsymbol{\Gamma}^{(k)})\mathbf{A}^{\mathrm{H}}\mathbf{C} + M^2Q^3L^4\mathbf{I}_{MQ}\big)\boldsymbol{\psi}^{(k)}. \tag{20}$$

The overall procedures for iterating the vector $\boldsymbol{\psi}$ are summarized in Algorithm 1, whose computational complexity is $\mathcal{O}(M^2Q^2L^2)$. To accelerate Algorithm 1, we can apply the square iterative methods [19] .

IV. Simulation Results

In our simulations, we first evaluate the ISL performance of our proposed design, and compare it to the existing schemes which include 'FHCS' [14], 'PBAL' [15], and 'POCS' [7]. Then, we evaluate the correlation levels of the FH waveforms generated by the aforementioned four methods including 'FHCS', 'PBAL', 'POCS', and our proposed design. Finally, we compare the symbol error rate (SER) performance of our proposed design with that of 'FHCS'. Throughout the simulations, we set the bandwidth and sampling frequency to be 150 MHz and 300 MHz, respectively. Moreover, we choose the absolute difference of the ISL values obtained at the current and previous iterations normalized by the initial one as the stopping criterion, whose tolerance is set to be 10^{-8}.

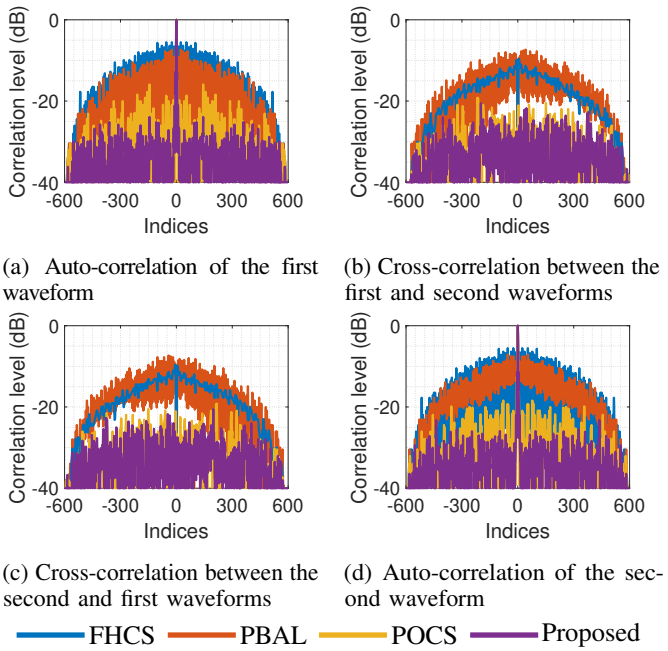

(a) Auto-correlation of the first waveform

(b) Cross-correlation between the first and second waveforms

(c) Cross-correlation between the second and first waveforms

(d) Auto-correlation of the second waveform

Fig. 1: Comparisons of FH waveform correlations between the tested methods.

In the first example, we evaluate the ISL values obtained by our proposed design and the other methods, including 'FHCS', 'PBAL', and 'POCS'. Different scenarios with varying numbers of waveforms $M \in \{2, 3, 4, 5\}$ and sub-pulses $Q \in \{15, 30, 60, 90\}$ are tested. The corresponding results, which are averaged over 20 independent trials, are shown in Table I. It can be seen that our proposed design achieves the lowest ISL values compared to the other tested methods in all considered scenarios, and the ISL differences become larger as the number of sub-pulses increases. For instance, in the case of $M = 3$ and $Q = 90$, the ISL value for our proposed design is around 15.06 dB, 8.41 dB, and 2.45 dB lower than 'FHCS', 'PBAL', and 'POCS', respectively. It verifies the capability of our proposed design in achieving low ISL values while implementing IE in the fast-time domain.

In the second example, we investigate the correlation levels of the FH waveforms generated by our proposed design, and compare them with the aforementioned existing methods. For all tested methods, the numbers of waveforms and sub-pulses are set to $M = 2$ and $Q = 100$, respectively. The corresponding results are shown in Fig. 1. It can be seen that the auto-

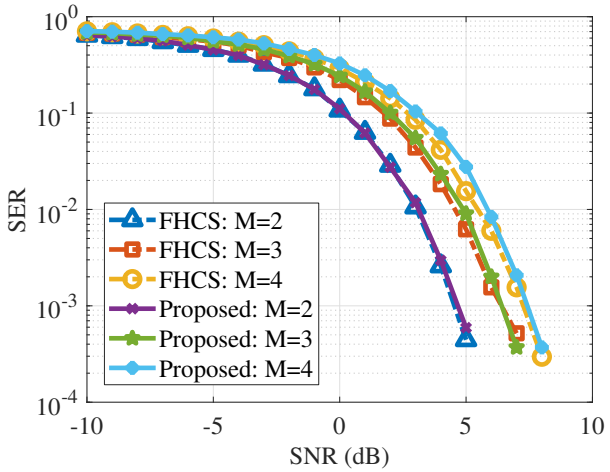

Fig. 2: SER performance comparisons of the tested methods.

and cross-correlations of our designed waveforms outperform those of the other three methods, which coincides with the ISL results in the first example. To be specific, the proposed design has reduced the worst auto-correlation level by 2.38 dB, 1.45 dB, and 1.24 dB compared to 'FHCS', 'PBAL', and 'POCS', respectively. In accordance, the highest cross-correlation level has been reduced by 10.93 dB, 13.21 dB, and 1.37 dB. These results further verify the effectiveness and superiority of our proposed design in improving the correlations of FH waveforms.

In the third example, we compare the SER performance of our proposed design with 'FHCS'. In this example, $M = 2$, 3, and 4 available waveforms are considered. We set the data rate to be 2 bits per sub-pulse, and also fix $N = 5$ and $Q = 90$ for all tested cases. We investigate the trends of the SER performance versus signal-to-noise ratio (SNR) values, and the corresponding results are shown in Fig. 2. It can be seen that the SER values decrease as the tested SNR values increase, and the SER performance of our proposed design is close to that of 'FHCS'. When $M = 3$ and the SNR value equals 5 dB, the difference in SER between our proposed method and 'FHCS' is 10^{-4}. Therefore, our proposed design with low ISL does not cause the degradation of SER performance.

V. CONCLUSION

We have developed an efficient multi-FH waveform design with good correlation properties and high-quality information transmission for the joint MIMO radar and communications. To facilitate the design, we have first built an appropriate model for FH waveforms. Then, we have exploited the frequency index modulation to implement fast-time IE, and have utilized the flexibility of initial phases of waveforms to reduce ISL. We have proposed the waveform design that minimizes ISL under constraints of IE and constant-modulus property, and have formulated it as a non-convex optimization problem. To obtain its closed-form solution at iterations, we have converted its objective function into a proper form using elementary algebraic properties, which has then been addressed by means of majorization-minimization technique. Simulation results have verified the effectiveness of our proposed waveform design and its superiority over the existing methods.

REFERENCES

[1] K. V. Mishra, M. R. Bhavani Shankar, V. Koivunen, B. Ottersten, and S. A. Vorobyov, "Toward millimeter-wave joint radar communications: A signal processing perspective," *IEEE Signal Process. Mag.*, vol. 36, no. 5, pp. 100–114, Sep. 2019.

[2] F. Liu, C. Masouros, A. P. Petropulu, H. Griffiths, and L. Hanzo, "Joint radar and communication design: Applications, state-of-the-art, and the road ahead," *IEEE Trans. Commun.*, vol. 68, no. 6, pp. 3834–3862, Jun. 2020.

[3] L. Zheng, M. Lops, Y. C. Eldar, and X. Wang, "Radar and communication coexistence: An overview: A review of recent methods," *IEEE Signal Process. Mag.*, vol. 36, no. 5, pp. 85–99, Sep. 2019.

[4] M. Bică and V. Koivunen, "Radar waveform optimization for target parameter estimation in cooperative radar-communications systems," *IEEE Trans. Aerosp. Electron. Syst.*, vol. 55, no. 5, pp. 2314–2326, Oct. 2019.

[5] K. Meng, C. Masouros, G. Chen, and F. Liu, "Network-level integrated sensing and communication: Interference management and BS coordination using stochastic geometry," *IEEE Trans. Wireless Commun.*, vol. 23, no. 12, pp. 19365–19381, Dec. 2024.

[6] L. M. Hoang, J. Andrew Zhang, D. N. Nguyen, and D. Thai Hoang, "Frequency hopping joint radar-communications with hybrid sub-pulse frequency and duration modulation," *IEEE Wireless Commun. Lett.*, vol. 11, no. 11, pp. 2300–2304, Nov. 2022.

[7] W. Baxter, E. Aboutanios, and A. Hassanien, "Joint radar and communications for frequency-hopped MIMO systems," *IEEE Trans. Signal Process.*, vol. 70, pp. 729–742, Jan. 2022.

[8] K. Wu, J. A. Zhang, X. Huang, and Y. J. Guo, "Frequency-hopping MIMO radar-based communications: An overview," *IEEE Aerosp. Electron. Syst. Mag.*, vol. 37, no. 4, pp. 42–54, Apr. 2022.

[9] D. Ma, N. Shlezinger, T. Huang, Y. Liu, and Y. C. Eldar, "FRaC: FMCW-based joint radar-communications system via index modulation," *IEEE J. Sel. Topics Signal Process.*, vol. 15, no. 6, pp. 1348–1364, Nov. 2021.

[10] M. -X. Gu, M. -C. Lee, Y. -S. Liu, and T. -S. Lee, "Design and analysis of frequency hopping-aided FMCW-based integrated radar and communication systems," *IEEE Trans. Wireless Commun.*, vol. 70, no. 12, pp. 8416-8432, Dec. 2022.

[11] Z. Xu and A. Petropulu, "A bandwidth efficient dual-function radar communication system based on a MIMO radar using OFDM waveforms," *IEEE Trans. Signal Process.*, vol. 71, pp. 401–416, Feb. 2023.

[12] I. P. Eedara, M. G. Amin, A. Hoorfar, and B. K. Chalise, "Dual-function frequency-hopping MIMO radar system with CSK signaling," *IEEE Trans. Aerosp. Electron. Syst.*, vol. 58, no. 3, pp. 1501–1513, Jun. 2022.

[13] X. Wang and A. Hassanien, "Phase modulated communications embedded in correlated FH-MIMO radar waveforms," in *Proc. IEEE Radar Conf.*, Florence, Italy, Sep. 2020, pp. 1–6.

[14] W. Baxter, E. Aboutanios, and A. Hassanien, "Dual-function MIMO radar-communications via frequency-hopping code selection," in *Proc. Asilomar Conf. Signals, Syst., Comput.*, Pacific Grove, CA, USA, Oct. 2018, pp. 1126–1130.

[15] E. Aboutanios, W. Baxter, and Y. D. Zhang, "Improved implementation of the frequency hopped code selection DFRC scheme," in *Proc. IEEE Radar Conf.*, San Antonio, TX, USA, May 2023, pp. 1–6.

[16] X. Xu, Y. Li, and R. Tao, "Information embedding design for the joint MIMO radar and communications via FH code selection," in *Proc. IEEE Wireless Commun. Netw. Conf. Workshops*, Nanjing, China, Mar. 2021, pp. 1–6.

[17] I. P. Eedara, M. G. Amin, and A. Hassanien, "Optimum code design using genetic algorithm in frequency hopping dual function MIMO radar communication systems," in *Proc. IEEE Radar Conf.*, Florence, Italy, Sep. 2020, pp. 1-6.

[18] Y. Li and S. A. Vorobyov, "Fast algorithms for designing unimodular waveform(s) with good correlation properties," *IEEE Trans. Signal Process.*, vol. 66, no. 5, pp. 1197–1212, Mar. 2018.

[19] R. Varadhan and C. Roland, "Simple and globally convergent methods for accelerating the convergence of any EM algorithm," *Scand. J. Statist.*, vol. 35, no. 2, pp. 335–353, 2008.